ChemComm

COMMUNICATION

View Article Online
View Journal | View Issue

Cite this: *Chem. Commun.*, 2015, **51**, 7919

Received 11th March 2015,
Accepted 1st April 2015

DOI: 10.1039/c5cc02058a

www.rsc.org/chemcomm

A hydrophobic adsorbent based on hierarchical porous polymers derived from morphologies of a biomineral†

Kosuke Sato, Yuya Oaki* and Hiroaki Imai*

The hierarchical porous structures of vinyl polymers, such as polystyrene (PSt) and poly(methyl methacrylate) (PMMA), were derived from morphologies of a biomineral through replication. The resultant PSt hierarchical structures showed enhanced adsorption properties of organic molecules as hydrophobic adsorbents in an aqueous medium.

Hierarchically organized structures in biominerals have relationships with their emergent properties, such as mechanical strength and optical properties.[1] Biomimetic approaches have been studied for the morphology control of crystalline materials.[2] However, it is not easy to achieve simultaneous synthesis and morphogenesis of such fine-tuned structures. If similar hierarchical morphologies are generated in a variety of materials, the enhanced properties can be derived from the morphology control. Here we report on the hierarchical morphology replication from a biomineral to vinyl polymers, such as polystyrene (PSt) and poly(methyl methacrylate) (PMMA). The porous PSt showed enhanced properties as a hydrophobic adsorbent originating from the replicated biogenic hierarchical morphologies with the micrometer-scale sponge structure and unit nanoparticles. Biominerals of calcium carbonate ($CaCO_3$) have a variety of morphologies consisting of the biological macromolecules and oriented calcite nanocrystals 20–100 nm in size.[3–5] Although biominerals are composed of abundant resources in nature, the hierarchically organized structures contribute to the emergence of the superior properties. Our challenge here is the application of the biogenic hierarchical structures to develop functional materials through morphology replication from biominerals to synthetic materials. The hierarchical structures of biominerals were used as the functional materials themselves, self-templates, and templates in previous studies.[6–9] For example, $CaCO_3$ biominerals themselves were applied to an adsorbent of gases and heavy metal ions and a stationary phase of chromatography.[6,7] The silica skeleton of a diatom served as the self-template for the preparation of a silicon hierarchical structure with enhanced electrochemical properties.[8] While biological resources were used as templates for synthesis and morphology control of inorganic materials,[9,10] the approaches were not fully applied to those of organic materials. Our group found that the hierarchical morphologies of biominerals and biomimetic materials were replicated to organic materials, such as conductive polymers and organic crystals.[11] However, the replicated hierarchical morphologies were not effectively applied for the enhancement of the properties. Our intention here is to find an application of the replicated polymer materials with the biogenic hierarchical morphologies.

Morphologies of polymer materials in a range of length scales are significant for their applications.[12] Syntheses of designed monomers and their precise polymerization direct morphology control of polymers at a molecular level.[13] Self-organized polymer materials in nanometer to micrometer scales are prepared by phase separation and segregation.[14] In general, it is not easy to achieve synthesis and simultaneous morphogenesis of polymers from nanometer to macroscopic scales. A variety of templates are used for morphogenesis of polymer materials from nanometer to micrometer scales, such as mesoscale porous materials, metal organic frameworks, and colloidal crystals of microparticles.[11,15–18] Electrospinning provides fibrous units of polymer materials to form the higher ordered structures.[19,20] However, generalizable methods for the hierarchical morphogenesis of polymer materials from nanoscopic to macroscopic scales are not fully studied in previous studies. We have proposed a method for synthesis and morphogenesis of conductive polymers through the replication of the original hierarchical structures in $CaCO_3$ biominerals.[11] Since a variety of hierarchical morphologies in $CaCO_3$ biominerals consist of the oriented nanocrystals,[3c] the incorporation and polymerization of the monomers in the interspace of the nanocrystals facilitate the morphogenesis of the polymers. The hierarchically organized polymer materials are obtained after dissolution of the original $CaCO_3$ materials. However, the method was only applied to oxidative polymerization of pyrrole and thiophene derivatives. In addition,

Department of Applied Chemistry, Faculty of Science and Technology, Keio University, 3-14-1 Hiyoshi, Kohoku-ku, Yokohama 223-8522, Japan. E-mail: oakiyuya@applc.keio.ac.jp, hiroaki@applc.keio.ac.jp

† Electronic supplementary information (ESI) available: Experimental methods, microscopy images, spectroscopic data, and data for adsorption experiments. See DOI: 10.1039/c5cc02058a

the replicated biogenic morphologies did not contribute to the enhancement of the properties in the previous reports.[11]

In the present work, we report on synthesis and morphogenesis of hierarchical porous polymers, such as PSt and PMMA, for a hydrophobic adsorbent. A sea urchin spine consisting of the micrometer scale sponge and unit nanoparticles was used as an original material for the morphology replication of the polymers. The biogenic structures were replicated to PSt and PMMA through radial polymerization of styrene (St) and methyl methacrylate (MMA) in the nanospace of the oriented unit crystals. The hierarchical morphologies of PSt contribute to the enhanced properties as a hydrophobic adsorbent. Macroscopic morphologies of PSt are controlled and designed in industrial scales for versatile uses. Recent reports showed the emergent properties originating from the morphology control of PSt.[20–22] Here we focused on a biogenic hierarchical architecture of a sea urchin spine with the micrometer-scale sponge morphology consisting of the oriented nanocrystals because the hierarchical morphologies combine to achieve the high specific surface area for the adsorption and permeability of an aqueous medium. Therefore, morphology replication provides PSt with the suitable structures as a hydrophobic adsorbent. The present work shows a new concept of the application of functional biogenic structures through the hierarchical morphology replication methods.

A sea urchin spine consisting of the oriented $CaCO_3$ nanocrystals and biological macromolecules was used as the original material for the hierarchical morphogenesis of PSt (Fig. 1a and b). The original sea urchin spine showed the sponge structure with continuous pores around 10 μm in diameter (Fig. 1a). The micrometer-scale sponge consisted of the oriented nanocrystals around 50 nm in size (Fig. 1b). The detailed experimental methods are described in the ESI.† The biological macromolecules incorporated into the nanospace were removed by the immersion in an aqueous solution containing sodium hypochlorite (NaClO) and subsequent heat treatment.

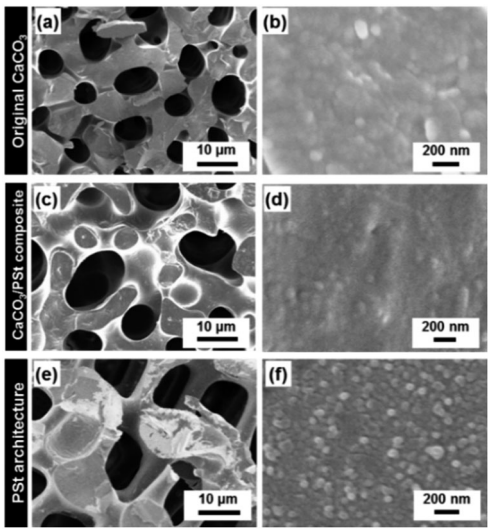

Fig. 1 Hierarchical morphology replication from a sea urchin spine as an original material to PSt. FESEM images of a sea urchin spine (a, b), the $CaCO_3$–PSt composites (c, d), and the PSt hierarchical architecture after dissolution of the original $CaCO_3$ material (e, f).

The neat liquid of the St monomer containing azobisisobutyronitrile (AIBN) as an initiator was introduced into the interspace of the nanocrystals. The $CaCO_3$ oriented nanocrystals containing the mixture of St and AIBN were maintained at 70 °C for 48 h. The AIBN concentration and polymerization temperature were referred to a previous work.[16b] After the radical polymerization proceeded, the composites of $CaCO_3$ and PSt were formed (Fig. 1c and d). The formation of PSt was confirmed by Fourier-transform infrared (FT-IR) spectroscopy (Fig. S1 in the ESI†). In the $CaCO_3$–PSt composites, PSt was not infiltrated into the micrometer-scale pores of the sponge structure (Fig. 1a and c).‡ The grain boundary of the nanocrystals was not clearly observed in the magnified image (Fig. 1d). The PSt content in the composites was estimated to be 8.7 wt% by thermogravimetric (TG) analysis (Fig. S2 in the ESI†). These results indicate that PSt was not formed in the micrometer-scale sponge pores but in the interspace of the unit nanocrystals. The incorporation and polymerization of the St monomer were achieved on the sponge skeletal body with a layer of around 10 μm in thickness. The control of the layer thickness was achieved in our previous work.[11a] The PSt hierarchical architecture was obtained by the dissolution of the original $CaCO_3$ material (Fig. 1e and f). The micrometer-scale sponge morphology consisted of nanoparticles around 70 nm in size. The replicated PSt showed a similar hierarchical structure to that of the original $CaCO_3$ material (Fig. 1a, b, e and f). In the PSt hierarchical architecture, the remaining calcium species originating from the original $CaCO_3$ material were not detected by energy dispersive X-ray (EDX) spectroscopy (Fig. S3 in the ESI†). In this way, the PSt hierarchical architecture was obtained through the morphology replication of a biomineral as an original material. Similar hierarchical morphologies of PMMA were obtained using the same method (Fig. S4 in the ESI†).

The incorporation and polymerization of the St monomer into the nanospace are the key processes for the hierarchical morphology replication. The bulk polymerization proceeds in the nanospace, even though the monomer and oligomers can remain in the polymerized material. Since PSt was formed and confined in the nanospace, the incorporated PSt showed different thermal properties from those of the bulk state on the thermograms of differential scanning calorimetry (DSC) (Fig. 2). The DSC thermogram of the

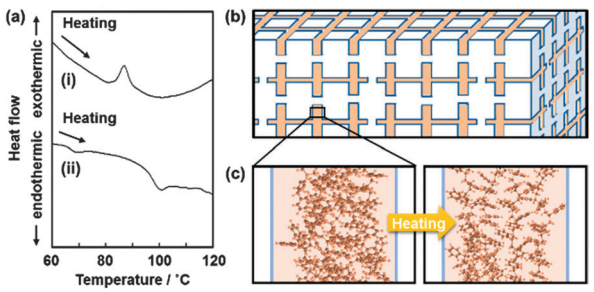

Fig. 2 Polymerization in the interspace of the oriented nanocrystals. (a) DSC curves of the $CaCO_3$–PSt composites (i) and bulk PSt synthesized under the same conditions without $CaCO_3$ (ii). (b) The schematic illustration of the incorporated PSt into the nanospace of the oriented unit crystals. (c) The schematic illustration of the incorporated PSt in the as-synthesized state (the left panel) and a stable conformation after the relaxation with an exotherm during the heating process.

$CaCO_3$–PSt composites showed the exothermic peak at around 85 °C during the heating process (chart (i) in Fig. 2a). The reference bulk PSt was synthesized using the same procedure in the absence of $CaCO_3$. The reference PSt showed the baseline shift with the endothermic peak at around 100 °C corresponding to the glass transition temperature (chart (ii) in Fig. 2a). In the $CaCO_3$–PSt composites, the exothermic peak at around 85 °C is ascribed to the conformational change in the PSt chains (Fig. 2b and c). Since PSt is synthesized from the neat liquid of St through radical polymerization in the confined nanospace, a stable conformation is not achieved in the as-synthesized state. Therefore, a stable conformation is achieved by the relaxation with an exotherm during the heating process (Fig. 2c). The same relaxation behavior was reported in PSt prepared in a metal organic framework.[16b] The results support that the formation of PSt proceeds not in the micrometer-scale sponge pores as the bulk state but in the confined nanospace (Fig. 2b).

Here the pore volume and pore diameter of the nanospace are estimated from the amount of PSt incorporated into the composite. Although a variety of organic compounds in liquid states have been introduced into the nanospace regardless of the hydrophilic and hydrophobic natures,[11] the pore volume and pore diameter of the nanospace are not estimated by a gas adsorption method. Since the $CaCO_3$–PSt composite includes 8.7 wt% of PSt in the nanospace (Fig. S2 in the ESI†), the volume of the incorporated PSt is calculated to be 9.16×10^{-2} cm^3 in 1 g of the original $CaCO_3$ oriented nanocrystals at a density of 1.04 g cm^{-3} for PSt. Therefore, the pore volume of the oriented nanocrystals (V_p) is estimated to be $V_p = 9.16 \times 10^{-2}$ cm^3 g^{-1} if the total volume of the nanospace, except the micrometer scale sponge pore (Fig. 1a), is occupied by PSt. When the shape and size of the $CaCO_3$ nanocrystals are assumed to be a cube of 50 nm on a side without aggregation (Fig. 1b), the specific surface area (S_{CaCO_3}) is estimated to be 44.3 m^2 g^{-1} at a density of 2.71 g cm^{-3} for $CaCO_3$. Based on these estimations, the pore width of the nanospace (L_p) is calculated to be L_p = 4.1 nm using eqn (1) based on the assumption that the space has a slit-type pore structure (Fig. 2b).[23]

$$L_p = \frac{2V_p}{S_{CaCO_3}} \quad (1)$$

The results support that the characteristic thermal properties as shown in Fig. 2 are ascribed to the confined effects in the nanospace corresponding to D_p = 4.1 nm. These results suggest that the oriented nanocrystals can be regarded as a family of porous materials.

The enhanced properties as a hydrophobic adsorbent were observed on the resultant hierarchical PSt architectures (Fig. 3). Rhodamine 6G and *p*-cresol were used as typical models of industrial wastewaters (Scheme S1 in the ESI†). The static adsorption properties were studied by changes in the initial concentrations (C_0) of rhodamine 6G and *p*-cresol. The aggregation of the nanoparticles around 200 nm in size, as a reference, was performed by reprecipitation of a commercial PSt from the toluene solution with the addition of methanol (Fig. S5 in the ESI†). The adsorption experiments were performed by immersion of the PSt samples in the aqueous solutions for 2 days. The aqueous solutions of rhodamine 6G and *p*-cresol penetrated into the hierarchical PSt (Fig. 3a). In contrast, the reprecipitated PSt floated on the aqueous solutions without the penetration even after 2 days (Fig. 3c). Since the concentrations of the remaining aqueous solutions became constant after 2 days, the adsorption equilibrium was assumed to be achieved. The adsorbed amounts (W) at the adsorption equilibrium concentrations (C_e) were measured after 2 days to prepare the adsorption isotherms (Fig. 3b and d). The relationship between the C_0, C_e, and W is summarized in Tables S1–S3 in the ESI.† Under all the experimental conditions, the hierarchical PSt showed the improved adsorption properties rather than the reprecipitated one (Fig. 3b and d). For example, the amount of the adsorbed rhodamine 6G was 253 mg g^{-1} for the hierarchical PSt at C_e = 0.444 wt% and 15.8 mg g^{-1} for the reprecipitated PSt at C_e = 0.484 wt% (Fig. 3b). The adsorption amount of the hierarchical PSt is comparable to 300 mg g^{-1} for that of a commercial PSt adsorbent (Amberlite XAD-2000) at C_e = 0.416 wt% (Table S1 and Fig. S6 in the ESI†). The amount of *p*-cresol adsorbed was 109 mg g^{-1} for the hierarchical PSt at C_e = 1.26 wt% and 23.7 mg g^{-1} for the reprecipitated PSt at C_e = 1.08 wt% (Fig. 3d). The amount is comparable to the adsorption amount of *m*-cresol on a porous PSt, namely 126 mg g^{-1} at C_e = 0.978 wt%, prepared by the flash freezing process, a new phase separation technique, in a recent report.[22]

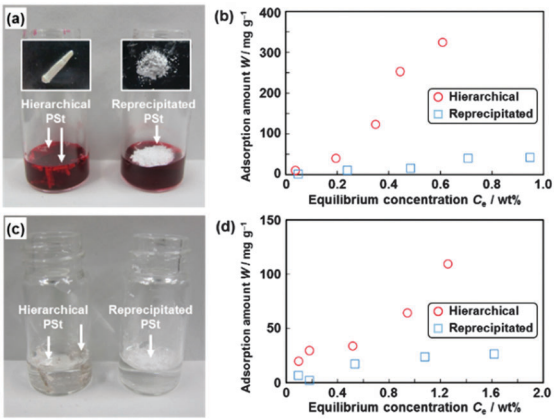

Fig. 3 Adsorption properties of rhodamine 6G (a, b) and *p*-cresol (c, d) on the PSt hierarchical architecture and reprecipitated PSt. (a, c) The photographs of the PSt hierarchical architecture and reprecipitated PSt immersed in the aqueous solutions of rhodamine 6G (a) and *p*-cresol (c). The insets of panel (a) show the pictures of the PSt samples before the adsorption experiments. (b, d) The adsorption isotherms of rhodamine 6G (b) and *p*-cresol (d) on the PSt hierarchical architecture (circles) and reprecipitated PSt (squares).§

The improved adsorption properties of the hierarchical PSt are ascribed to the morphologies replicated from a sea urchin spine (Fig. 1e and f). The sponge morphology of PSt at a micrometer scale contributes to the permeability of the aqueous solutions. The unit nanoparticles around 70 nm in diameter serve as the adsorption site with a high specific surface area. The specific surface area of the PSt spheres (S_{PSt}) is estimated to be 82.4 m^2 g^{-1} when the density and diameter of PSt are assumed to be 1.04 g cm^{-3} and 70 nm, respectively. Around C_e = 1 wt%, the number of cresol molecules on 1 nm^2 of the PSt samples (n_c) was calculated to be 4.49 nm^{-2} for our hierarchical PSt, 2.50 nm^{-2} for a commercial one (Amberlite XAD-200), and 3.79 nm^{-2} for a porous PSt in a previous

report.[22] The resultant hierarchical PSt showed the highest n_c rather than the reference adsorbent samples. These results suggest that the replicated biogenic hierarchical morphologies on PSt possess a suitable structure for a hydrophobic adsorbent.

In summary, the hierarchical morphologies of a sea urchin spine, a biological resource, are replicated to PSt and PMMA. The original sea urchin spine consisted of the micrometer-scale sponge morphology and oriented nanocrystals. The hierarchical morphology replication was achieved by the incorporation and polymerization of the monomers in the interspace of the oriented nanocrystals. Since PSt was synthesized in the confined nanospace, the unique exothermic behavior with the conformational changes was observed on the DSC thermogram. The results indicate that the interspace of the oriented nanocrystal was a confined nanospace. The hierarchical PSt showed enhanced adsorption properties as a hydrophobic adsorbent. The enhancement of the adsorption properties is ascribed to the hierarchical structures including the micrometer-scale pores of the sponge morphology and interspace of the nanoparticles. The present work is a model case of using a sea urchin spine. Functional morphologies of biological resources have potential for the enhancement of the properties in a variety of materials. The present method for the hierarchical morphology replication can be applied to the development of a variety of functional polymer materials.

Notes and references

‡ A sea urchin spine consisting of the oriented $CaCO_3$ nanocrystals was immersed in a neat liquid of the monomers. Then, the excess monomer, such as in the micrometer-scale pores of the sponge, was absorbed by a paper towel. As reported in our previous studies,[11] the method facilitates the incorporation of the monomers into the nanospace without the infiltration of the micrometer-scale pore. The monomer-incorporated sample was set in a vessel with the other vessel containing the monomer. Since the monomer vapor was filled in the reaction chamber, the incorporated monomer was not easily vaporized from the nanospace.
§ The adsorption isotherms of the commercial PSt adsorbent are displayed in Fig. S6 in the ESI.†

1 (*a*) S. Mann, in *Biomineralization Principles and Concepts in Bioinorganic Materials Chemistry*, ed. R. G. Compton, S. G. Davies and J. Evans, Oxford University Press, Oxford, 2001; (*b*) S. Weiner and L. Addadi, *J. Mater. Chem.*, 1997, **7**, 789; (*c*) T. Kato, *Adv. Mater.*, 2000, **12**, 1543.
2 (*a*) S. Mann, *Nature*, 1988, **332**, 119; (*b*) T. Kato, A. Sugawara and N. Hosoda, *Adv. Mater.*, 2002, **14**, 869; (*c*) S.-H. Yu and H. Cölfen, *J. Mater. Chem.*, 2004, **14**, 2124; (*d*) H. Imai, Y. Oaki and A. Kotachi, *Bull. Chem. Soc. Jpn.*, 2006, **79**, 1834; (*e*) A.-W. Xu, Y. Ma and H. Cölfen, *J. Mater. Chem.*, 2007, **17**, 415; (*f*) F. C. Meldrum and H. Cölfen, *Chem. Rev.*, 2008, **108**, 4332; (*g*) N. A. J. M. Sommerdijk and G. de With, *Chem. Rev.*, 2008, **108**, 4499; (*h*) T. Kato, T. Sakamoto and T. Nishimura, *MRS Bull.*, 2010, **35**, 127.
3 (*a*) Y. Oaki and H. Imai, *Angew. Chem., Int. Ed.*, 2005, **44**, 6571; (*b*) Y. Oaki and H. Imai, *Small*, 2006, **2**, 66; (*c*) Y. Oaki, A. Kotachi, T. Miura and H. Imai, *Adv. Funct. Mater.*, 2006, **16**, 1633.
4 (*a*) K. Takahashi, H. Yamamoto, A. Onoda, M. Doi, T. Inaba, M. Chiba, A. Kobayashi, T. Taguchi, T. Okamura and N. Ueyama, *Chem. Commun.*, 2004, 996; (*b*) I. Sethmann, A. Putnis, O. Gransmann and P. Löbmann, *Am. Mineral.*, 2005, **90**, 1213.
5 H. Cölfen and M. Antonietti, *Mesocrystals and Nonclassical Crystallization*, John Wiley & Sons, 2008.
6 (*a*) S. Yamanaka, T. Oiso, Y. Kurahashi, H. Abe, K. Hara, T. Fujimoto and Y. Kuga, *J. Nanopart. Res.*, 2014, **16**, 2266; (*b*) Z. Zhao, L. Zhang, H. Dai, Y. Du, X. Meng, R. Zhang, Y. Liu and J. Deng, *Microporous Mesoporous Mater.*, 2011, **138**, 191; (*c*) G. B. Cai, G. X. Zhao, X. K. Wang and S. H. Yu, *J. Phys. Chem. C*, 2010, **114**, 12948; (*d*) S. Chowdhury and P. Saha, *Chem. Eng. J.*, 2010, **164**, 16; (*e*) X. Q. Li, Z. Feng, Y. Xia and H. C. Zeng, *Chem. – Eur. J.*, 2012, **18**, 1945.
7 K. Sato, Y. Oaki, D. Takahashi, K. Toshima and H. Imai, *Chem. – Eur. J.*, 2015, **21**, 5034.
8 (*a*) C. S. Gaddis and K. H. Sandhage, *J. Mater. Res.*, 2004, **19**, 2541; (*b*) H. Zhou, T. Fan, X. Li, J. Ding, D. Zhang, X. Li and Y. Gao, *Eur. J. Inorg. Chem.*, 2009, 211; (*c*) J. Toster, K. Iyer, W. Xiang, F. Rosei, L. Spiccia and C. Raston, *Nanoscale*, 2012, **5**, 873.
9 (*a*) R. Seshadri and F. C. Meldrum, *Adv. Mater.*, 2000, **12**, 1149; (*b*) E. Payne, N. Rosi, C. Xue and C. Mirkin, *Angew. Chem., Int. Ed.*, 2005, **44**, 5064; (*c*) Y. Zhang, Y. Liu, X. Ji, C. E. Banks and W. Zhang, *J. Mater. Chem.*, 2011, **21**, 14428; (*d*) H. Yao, G. Zheng, W. Li, M. McDowell, Z. Seh, N. Liu, Z. Lu and Y. Cui, *Nano Lett.*, 2013, **13**, 3385.
10 (*a*) P. Greil, *MRS Bull.*, 2010, **35**, 145; (*b*) S. Hall, H. Bolger and S. Mann, *Chem. Commun.*, 2003, 2784; (*c*) W. Zhang, D. Zhang, T. Fan, J. Gu, J. Ding, H. Wang, Q. Guo and H. Ogawa, *Chem. Mater.*, 2009, **21**, 33.
11 (*a*) Y. Oaki, M. Kijima and H. Imai, *J. Am. Chem. Soc.*, 2011, **133**, 8594; (*b*) M. Kijima, Y. Oaki, Y. Munekawa and H. Imai, *Chem. – Eur. J.*, 2013, **19**, 2284; (*c*) Y. Munekawa, Y. Oaki and H. Imai, *Langmuir*, 2014, **30**, 3236; (*d*) R. Muramatsu, Y. Oaki, K. Kuwabara, K. Hayashi and H. Imai, *Chem. Commun.*, 2014, **50**, 11840; (*e*) Y. Munekawa, Y. Oaki, K. Sato and H. Imai, *Nanoscale*, 2015, **7**, 3466.
12 (*a*) T. Kelly and M. Wolf, *Chem. Soc. Rev.*, 2010, **39**, 1526; (*b*) H. Hentze, *Curr. Opin. Solid State Mater. Sci.*, 2001, **5**, 343; (*c*) Q. Wei and S. James, *Chem. Commun.*, 2005, 1555; (*d*) C. Martin, *Acc. Chem. Res.*, 1995, **28**, 6168.
13 (*a*) M. Kamigaito, T. Ando and M. Sawamoto, *Chem. Rev.*, 2001, **101**, 3689; (*b*) S. Aoshima and S. Kanaoka, *Chem. Rev.*, 2009, **109**, 5245; (*c*) E. Yashima, K. Maeda, H. Iida, Y. Furusho and K. Nagai, *Chem. Rev.*, 2009, **109**, 6102.
14 (*a*) T. Kato, N. Mizoshita and K. Kishimoto, *Angew. Chem., Int. Ed.*, 2006, **45**, 38; (*b*) A. R. Murphy and J. M. J. Fréchet, *Chem. Rev.*, 2007, **107**, 1066; (*c*) T. Aida, E. W. Meijer and S. I. Stupp, *Science*, 2012, **335**, 813; (*d*) J. J. L. M. Comelissen, A. E. Rowan, R. J. M. Nolte and N. A. J. M. Sommerdijk, *Chem. Rev.*, 2001, **101**, 4039; (*e*) Y. Mai and A. Eisenberg, *Chem. Soc. Rev.*, 2012, **41**, 5969.
15 (*a*) T. Bein and P. Enzel, *Angew. Chem., Int. Ed. Engl.*, 1989, **28**, 1692; (*b*) D. J. Cardin, *Adv. Mater.*, 2002, **14**, 553; (*c*) K. Tajima and T. Aida, *Chem. Commun.*, 2000, 2399; (*d*) R. A. Caruso and M. Antonietti, *Chem. Mater.*, 2001, **13**, 3272.
16 (*a*) T. Uemura, S. Horike, K. Kitagawa, M. Mizuno, K. Endo, S. Bracco, A. Comotti, P. Sozzani, M. Nagaoka and S. Kitagawa, *J. Am. Chem. Soc.*, 2008, **130**, 6781; (*b*) T. Uemura, T. Kaseda and S. Kitagawa, *Chem. Mater.*, 2013, **25**, 3772.
17 (*a*) S. Horike, S. Shimomura and S. Kitagawa, *Nat. Chem.*, 2009, **1**, 695; (*b*) T. Uemura, N. Yanai and S. Kitagawa, *Chem. Soc. Rev.*, 2009, **38**, 1228.
18 (*a*) A. Thomas, F. Goettmann and M. Antonietti, *Chem. Mater.*, 2008, **20**, 738; (*b*) S. Moon and T. McCarthy, *Macromolecules*, 2003, **36**, 4253; (*c*) S. Chakraborty, Y. Colón, R. Snurr and S. Nguyen, *Chem. Sci.*, 2015, **6**, 384; (*d*) V. Cepak and C. Martin, *Chem. Mater.*, 1999, **11**, 1363; (*e*) P. Sozzani, S. Bracco, A. Comotti, R. Simonutti, P. Valsesia, Y. Sakamoto and O. Terasaki, *Nat. Mater.*, 2006, **5**, 545.
19 (*a*) N. Zander, *Polymers*, 2013, **5**, 19; (*b*) S. Agarwal, A. Greiner and J. Wendorff, *Prog. Polym. Sci.*, 2013, **38**, 963; (*c*) A. Frenot and I. Chronakis, *Curr. Opin. Colloid Interface Sci.*, 2003, **8**, 64.
20 (*a*) J. Lin, F. Tian, Y. Shang, F. Wang, B. Ding, J. Yu and Z. Guo, *Nanoscale*, 2013, **5**, 2745; (*b*) X. Li, B. Ding, J. Lin, J. Yu and G. Sun, *J. Phys. Chem. C*, 2009, **113**, 20452.
21 (*a*) L. Jiang, Y. Zhao and J. Zhai, *Angew. Chem., Int. Ed.*, 2004, **43**, 4338; (*b*) Y. Lu, Y. Yin, Z.-Y. Li and Y. Xia, *Langmuir*, 2002, **18**, 7722; (*c*) M. Kaliva, G. Armatas and M. Vamvakaki, *Langmuir*, 2012, **28**, 2690; (*d*) P. Jing, X. Fang, J. Yan, J. Guo and Y. Fang, *J. Mater. Chem. A*, 2013, **1**, 10135.
22 (*a*) S. Samitsu, R. Zhang, X. Peng, M. Krishnan, Y. Fujii and I. Ichinose, *Nat. Commun.*, 2013, **4**, 2356; (*b*) M. Krishnan, S. Samitsu, Y. Fujii and I. Ichinose, *Chem. Commun.*, 2014, **50**, 9393.
23 K. Kaneko and C. Ishii, *Colloids Surf.*, 1992, **67**, 203.

